Journal of Physics D: Applied Physics

PAPER

Radiation sensors based on GaN microwires

To cite this article: D Verheij *et al* 2018 *J. Phys. D: Appl. Phys.* **51** 175105

IOP Publishing Journal of Physics D: Applied Physics

J. Phys. D: Appl. Phys. **51** (2018) 175105 (10pp) https://doi.org/10.1088/1361-6463/aab636

Radiation sensors based on GaN microwires

D Verheij[1,2], M Peres[1,2], S Cardoso[2], L C Alves[3], E Alves[1], C Durand[4], J Eymery[5] and K Lorenz[1,2]

[1] IPFN, Instituto Superior Técnico, Campus Tecnológico e Nuclear, Bobadela LRS, Portugal
[2] Instituto Superior Técnico and Instituto de Engenharia de Sistemas de Computadores—Microsystems and Nanotechnology (INESC-MN), Lisboa, Portugal
[3] C2TN, Instituto Superior Técnico, Campus Tecnológico e Nuclear, Bobadela LRS, Portugal
[4] CEA INAC-Pheliqs-NPS, Université Grenoble Alpes, Grenoble, France
[5] CEA INAC-MEM-NRS, Université Grenoble Alpes, Grenoble, France

E-mail: dirkjanverheij@ctn.tecnico.ulisboa.pt and lorenz@ctn.tecnico.ulisboa.pt

Received 11 December 2017, revised 5 March 2018
Accepted for publication 13 March 2018
Published 10 April 2018

Abstract

GaN microwires were shown to possess promising characteristics as building blocks for radiation resistant particle detectors. They were grown by metal organic vapour phase epitaxy with diameters between 1 and 2 μm and lengths around 20 μm. Devices were fabricated by depositing gold contacts at the extremities of the wires using photolithography. The response of these single wire radiation sensors was then studied under irradiation with 2 MeV protons. Severe degradation of the majority of devices only sets in for fluences above 4×10^{16} protons cm^{-2} revealing good radiation resistance. During proton irradiation, a clear albeit small current gain was observed with a corresponding decay time below 1 s. Photoconductivity measurements upon irradiation with UV light were carried out before and after the proton irradiation. Despite a relatively low gain, attributed to significant dark currents caused by a high dopant concentration, fast response times of a few seconds were achieved comparable to state-of-the-art GaN nanowire photodetectors. Irradiation and subsequent annealing resulted in an overall improvement of the devices regarding their response to UV radiation. The photocurrent gain increased compared to the values that were obtained prior to the irradiation, without compromising the decay times. The results indicate the possibility of using GaN microwires not only as UV detectors, but also as particle detectors.

Keywords: GaN, microwires, radiation detectors, photoconductivity, ion beam induced conductivity, proton irradiation

(Some figures may appear in colour only in the online journal)

1. Introduction

GaN is a wide direct bandgap semiconductor and has been applied in high efficiency ultraviolet (UV) light-emitting and sensing applications since the nineties [1, 2]. More recently, its nano- and microwire configurations have attracted intense attention for application in UV photodetectors due to their high crystal quality and high surface to volume ratio [3, 4].

Two relevant parameters to create commercially interesting sensors are gain and response time. In comparison to their bulk counterparts, GaN nanowire-based photodetectors have achieved higher photoconductive gain [3]. Nonetheless, these devices also present limitations such as limited temperature stability [1] as well as the existence of a persistent photocurrent (PPC), i.e. an increased current level that persists even when the external stimulus is switched off [4], which leads to long decay times. In general, in nanowire sensors, a fundamental trade-off between the photoconductive gain and speed of photodetectors exists, as the increase of one of these parameters usually decreases the other [5]. Furthermore, when assembling a device, special care must be taken when depositing the contacts as typically processing will modify

surface state properties, which can harm the reproducibility characteristics of the radiation sensors [6]. Recently, efficient UV detection based on InGaN/GaN coreshell microwires was demonstrated including the possibility of integrating these devices in flexible substrates [7, 8].

The potential of GaN nano- and microwires as a base material for photodetectors has already been demonstrated; however, no reports exist on their sensing capabilities for heavy particles such as protons, neutrons and ions. Ion beam induced conductivity was measured in zinc oxide nanowires. Devices containing wires with diameters between 150 and 250 nm were irradiated with He^+ ions while measuring their conductance at constant bias [9]. It is therefore desirable to extend the characterization of GaN microwire radiation sensors to irradiation with heavy particles. The assembly of such a device can potentially fill the gap that currently exists.

Particle detectors based on GaN thin films, on the other hand, have been successfully realized. Polyakov *et al* [10] and Xu *et al* [11] were able to successfully detect α-particles using a Schottky structure while Vaitkus *et al* [12] achieved similar results with ohmic behaviour. GaN is an interesting material to be applied in high energy radiation detectors because, beside its wide bandgap, it also possesses a large displacement energy, high thermal stability, as well as strong defect mobility at room temperature, leading to dynamic annealing during irradiation, which make GaN a radiation hard medium [13, 14]. This property is especially important in harsh environments, where high temperatures and energy deposition can cause the rapid degradation of the standard materials used for detectors, such as silicon. The radiation hardness of GaN films to proton and neutron radiation was studied by Grant *et al* [15] and they point out a number of issues, mainly related to the thickness of available material and large density of defects produced during the growth process. These defects are mainly related to the lattice and thermal expansion mismatch between GaN and the sapphire substrate. Other groups also reported that the high dislocation densities in GaN heteroepitaxial films limit carrier mobility and increase leakage currents [16, 17]. Using microwires can solve these problems to a great extent as defect densities produced due to the lattice mismatch are significantly reduced. GaN microwires can be considered as almost dislocation free along their length because lattice-mismatch (misfit) dislocations occurring at the Al_2O_3/GaN interface are bent to the sidewall surface very close to the bottom of the wire [18]. On the other hand, inversion domains are frequently observed [19] and stacking faults have been reported at the interface between doped and nominally undoped parts [18].

The improved crystalline quality of dislocation free microwires is expected to decrease leakage currents compared to thin film devices. Additionally, compared to nanowires, the larger volume of microwires makes them better suited for the detection of high energy particles and x-rays. In this way, the idea is to settle a compromise between the better crystalline quality associated to wire-based GaN and the larger volume of GaN layers. However, surface defects are often seen to dominate the behaviour of nanowire devices due to Fermi level pinning at the surface. This leads to surface band bending and the formation of a depletion region at the nanowire surface. Indeed, a detailed study of the influence of the nanowire diameter on UV detection, for nanowires grown by molecular beam epitaxy, showed that Fermi level pinning yields a full depletion of nanowires with small diameters explaining high gains and fast response. However, above a critical diameter of $\sim$80 nm, a conductive core is maintained and devices show higher dark currents, a lower gain and stronger persistent currents [20]. In particular, the surface band bending causes the separation of irradiation induced electrons and holes which then suppresses their recombination when the irradiation is switched off leading to persistent current. Nevertheless, this effect should be much smaller in heavily doped wires like those used in the present study. Indeed, our results suggest that the behaviour of the microwire devices discussed here is quasi-bulk, i.e. surface defects do not play a major role in the observed response of the radiation sensors.

2. Experimental methods

GaN wires were grown by catalyst-free metal organic vapour phase epitaxy (MOVPE) as reported previously [21]. The c-plane sapphire substrate is first baked *in situ* under H_2 at 1040 °C and nitridated with NH_3 (2000 sccm) for 30 s to form a thin AlN surface layer. Then, by injecting simultaneously SiH_4 (45 sccm) and NH_3 (4000 sccm) for 100 s a SiN_x layer is deposited. Following these steps, the GaN seed nucleation is achieved at 1000 °C by injecting the respective precursors, trimethylgallium (TMG) (135 μmol min^{-1}) and NH_3 (2.232 mmol min^{-1}), into the chamber under a N_2 carrier gas flow. The vertical growth is initiated immediately after seed nucleation keeping the same temperature and small V/III molar ratio but with an additional injection of silane (200 nmol min^{-1}). The silane flux is fundamental to initiate the vertical growth of long wires by MOVPE as reported in [21]. When the wires are approximately 13 μm long, the silane flux is turned off and vertical growth continues for approximately another 7 μm.

The resulting microwires present diameters ranging from 1 μm to 2 μm and a length of approximately 20 μm. The silane flux causes the incorporation of Si donors into the bottom part of the grown wires, leading to a highly doped section with a doping concentration in the 10^{19}–10^{20} cm^{-3} range. Additionally, due to the silane, a thin shell (<3 nm) of SiN_x is formed around this part of the wire. In the upper part, since no silane flux was used during growth, unintentionally doped n-type GaN, with a lower carrier concentration ($\sim 10^{18}$ cm^{-3}) [22], is grown and no SiN_x sidewall layer exists [23]. As will be demonstrated in the following section, this discontinuity in the doping concentration will influence the electrical properties of the devices.

A full description of the growth process can be found in [21]. A bird-view scanning electron microscopy (SEM) image of the as-grown microwires is shown in figure 1(a) accompanied by a schematic in figure 1(b). They are single crystals and essentially dislocation free as demonstrated by high resolution transmission electron microscopy [8] and are in a well-defined epitaxial relationship with sapphire ($[1\,\bar{1}\,0\,0]_{GaN}$ // $[1\,\bar{2}\,1\,0]_{Sapp}$

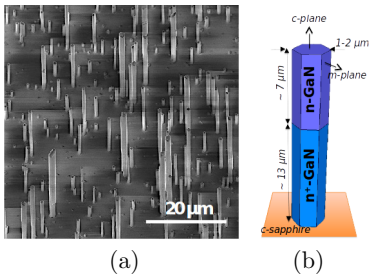

(a) (b)

Figure 1. (a) SEM image with a magnification of 901× of the as-grown microwires; (b) schematic of a single microwire (not on scale).

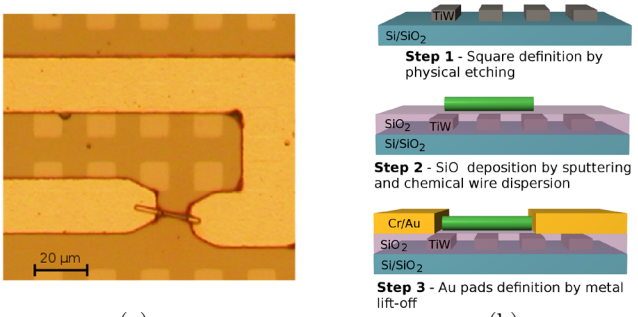

(a) (b)

Figure 2. (a) Optical microscopy image of a microwire device after the lift-off step. The squares of the grid have a lateral size of 10 μm and the width of the contact paths is 20 μm. (b) Schematic representation (not on scale) of the three fabrication steps: metal grid definition by physical etching of the TiW layer on silicon, SiO_2 deposition by sputtering and wire dispersion, and Cr/Au pads definition by metal lift-off.

and $[0\,0\,0\,1]_{GaN}$ // $[0\,0\,0\,1]_{Sapp}$ within less than one degree of twist and tilt) [21]. The crystalline quality has also been demonstrated recently by nanoprobe coherent x-ray diffraction very sensitive to all structural defects revealing that the main defects are inversion domain boundaries i.e. the coexistence of domains of different polarity [19].

To fabricate the radiation sensors, a methodology consisting of three main phases was followed. Firstly, with the knowledge that the placement of the microwires by dispersion on a substrate is random, a grid needs to be deposited. Thus a TiW metal grid consisting of an array of 10×10 μm^2 squares was deposited on the silicon substrate and subsequently covered by SiO_2. The way this grid will aid to locate the microwires is as follows. Each small square represents a position (defined by a set of coordinates) in the matrix of squares. After the dispersion of the microwires, the sample is inspected with an optical microscope and the location of single microwires is defined according to the coordinates of the grid. These coordinates then define the location to deposit the metal contacts by a further lithography step. In detail, the structure of the grid consists of 150 Å thick TiW squares, deposited on top of silicon covered by a thin oxide layer due to the exposure of the wafer to ambient conditions. To draw the desired pattern, photolithography was done with a Direct Write Laser Heidelberg 2.0 system and, finally, to avoid contact between the wires and the TiW, an insulating layer of 2000 Å SiO_2 was deposited in a Alcatel SCM 450 sputtering system. The conditions for this deposition were a RF power of 190 W, a pressure of 4 mTorr and a deposition rate of 11.97 Å min^{-1}. The second stage is the dispersion of the microwires. This was done by primarily detaching them from their Al_2O_3 growth substrate via ultrasound treatment for 15 minutes. Afterwards, some droplets of the resulting suspension of microwires in isopropyl alcohol were deposited on the SiO_2. By optical microscopy and with the grid as a reference, their position was defined. In the third step, a metal lift-off process was used to deposit the contacts. Contact paths were drawn using photolithography, which was followed by the deposition of 300 Å of Cr and 4000 Å of Au by magnetron sputtering in a Alcatel SCM 450 machine. The conditions for this deposition were an RF power of 200 W, a pressure of 3‘mTorr and a deposition rate of 55.6 Å min^{-1}. The lift-off was achieved by immersing the substrate into a microstrip solution which was then placed, subsequently, in a heat bath (60 °C) and in an ultrasound bath (60 °C) for 4 h. Finally, the substrates were integrated on a chip carrier in order to allow *in situ* measurements while performing proton irradiation. Figure 2 shows an optical microscopy image of a single sensor that was successfully fabricated as well as a schematic of the device processing steps.

Electrical and opto-electrical characterization were performed using a two-probe configuration, connected to an Agilent B1500A semiconductor device analyser. For the photoconductivity measurements a high-power UV LED with a dominant wavelength of 365 nm and with a typical output power of 360 mW was used. Excitation energy dependence, gain and decay time of the photocurrent were studied through photoconductivity spectroscopy, steady-state I–V and transient I–V measurements, respectively [24].

The proton irradiation was carried out at the nuclear microprobe facility at IST/LATR. The energy of the proton beam used in the experiments is 2 MeV and during the measurements, the beam area was set to 20×20 μm^2 and the current to 300 pA, which corresponds to a flux of 5×10^{14} protons (cm^{-2} s^{-1}). This flux was maintained during the entire proton irradiation experiment. The fluence is then calculated by multiplying this flux by the irradiation time. It should be noted that the focused beam is quite intense leading to high fluences in just few minutes of irradiation i.e. for the highest fluence of 1.2×10^{17} protons cm^{-2} only four minutes of irradiation were required. Taking into account the surface area of the microwires, which is obtained by multiplying their diameter and length, approximately 10^8 protons impact a single wire each second. The main goals of the measurements are to analyse how the wires react to the proton irradiation in terms of induced conductivity but also to see how the wires are affected in terms of defect creation. SRIM simulations (stopping and ranges of ions in matter) [25] for a 2 MeV proton beam on a planar GaN substrate, using displacement energies of 45 eV and 109 eV for Ga and N respectively [26], yield a projected range of ~24 μm and suggest that we can safely assume that no hydrogen implantation occurs. Although slight discrepancies are expected due to the non-planar nature of the microwire samples, the simulations indicate that the ionization profile will be constant across the entire microwire cross-section (see

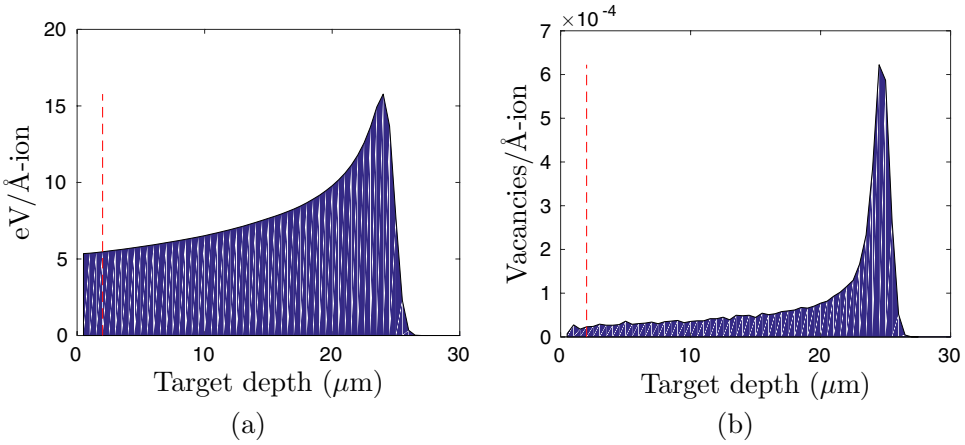

Figure 3. SRIM simulation for 2 MeV protons hitting a planar GaN target. The red dashed line represents the depth corresponding to a typical GaN microwire diameter; (a) the energy loss due to ionization plotted versus the target depth; (b) number of vacancies plotted versus the target depth.

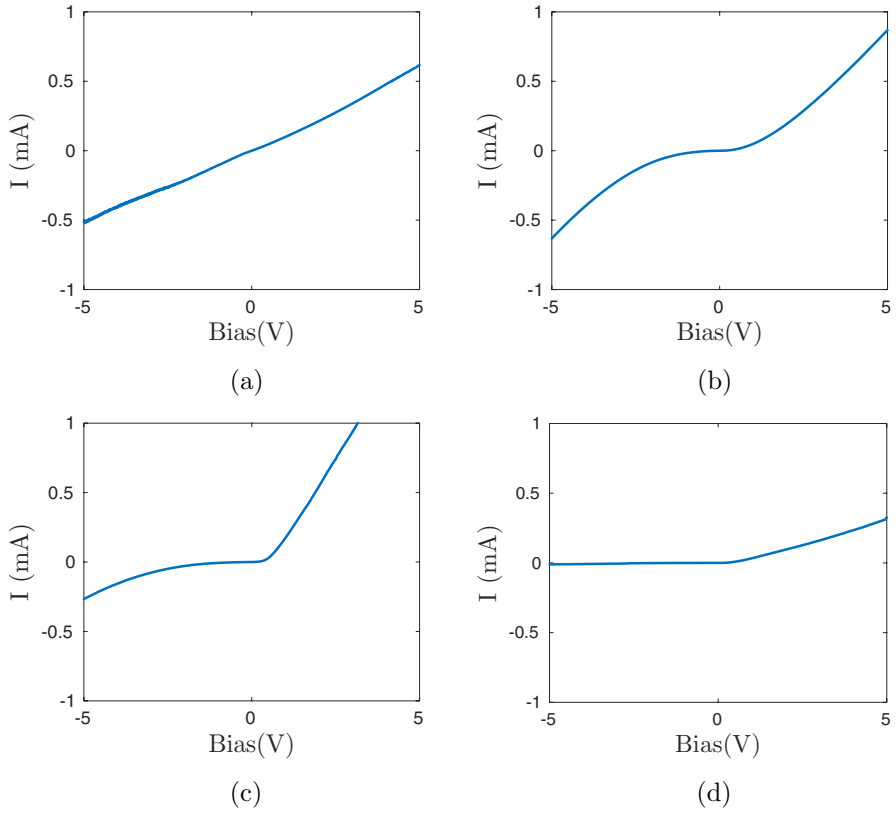

Figure 4. Experimental I–V curves obtained for four different samples. The I–V characteristics are (a) almost linear (129D), (b) almost symmetric (102U), (c) asymmetric (216U) and (d) rectifying (326D).

figure 3(a)). Finally, the plot relative to the collision events, shows that there will be some damage creation, but since the protons cross the wires, the number of created defects will not be large (see figure 3(b)).

3. Results and discussion

3.1. Electrical characterization

The I–V measurements showed that not all the devices presented identical I–V behaviour. We can divide the results into four types of curves: almost linear (figure 4(a)), almost symmetric (figure 4(b)), asymmetric (figure 4(c)) and rectifying (figure 4(d)). The most commonly obtained curves (18 out of 23) are almost symmetric or asymmetric. However, after annealing the devices at 400° for 60 s, the almost symmetric curves tended to become more asymmetric, while the asymmetric curves were not altered. The reason devices fabricated in the same way present different responses is probably due to unavoidable processes that occur during fabrication which may alter the metal-semiconductor interface properties. Additionally, the oxidation of the GaN surface, which can

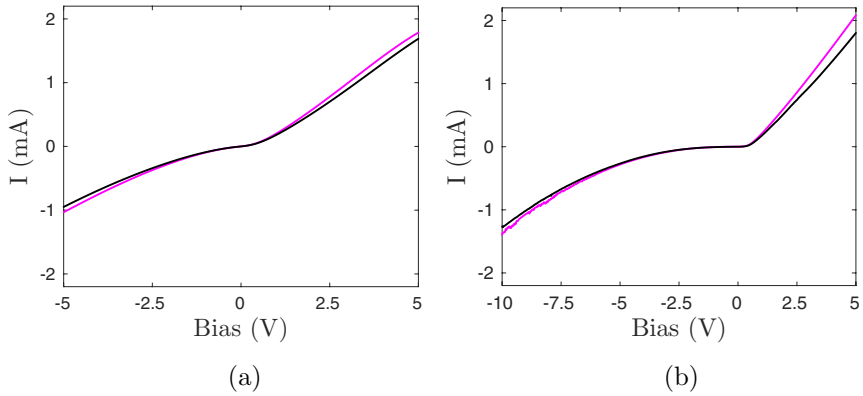

Figure 5. I–V characteristics of the devices 105U (a) and 216U (b) measured under dark (black curve) conditions and when irradiated with the high-power UV LED (magenta curve).

be inhomogeneous from wire to wire might also influence the contact properties. The polarisation inversion domains observed in these microwires [19] may also contribute to distinct I–V characteristics from wire to wire. In GaN layers they were suggested to modify the transport properties across Schottky barriers [27]. Similar results were also obtained by Zhang *et al* when performing electrical measurements on Bi_2S_3 nanowires and attributed to variations of the intrinsic parameters of the nanowires and to different contact geometries and properties such as the contact area and Schottky barrier height [28]. In the present case, the asymmetry in the I–V curves can be attributed to the discontinuity of charge carriers along the microwire due to the doping profile. As is well known, the thickness of the depletion width is proportional to the inverse square root of the donor concentration (N_d) [29]. Thus, for a higher N_d the tunnelling of electrons through the barrier becomes more significant, yielding a higher current. Consequently, for the highly doped end a more ohmic like contact is expected while for the top of the wire, the type of contact depends on whether the doping concentration is or not below the semiconductor metal transition. As said, in our samples mostly Schottky contacts were obtained for the moderately doped section. It is also important to notice that the devices present high dark conductivity, in agreement with the high Si doping level. Microwires grown by an identical process as those used in this investigation but with a homogeneous high doping concentration along the wire axis were studied by Tchoulfian *et al* [30, 31] and they also reported a very high conductivity and estimated carrier concentrations above 10^{20} cm^{-3}.

3.2. Photoconductivty

To study the photoconductive properties of the devices, spectroscopy, static I–V and transient I–V measurements upon irradiation with light were performed. As expected, photoconductivity spectra showed that the photocurrent is low for excitation below the bandgap and absorption increases for wavelengths close to the bandgap for all tested devices (not shown).

In figures 5(a) and (b) I–V curves obtained during irradiation with the UV LED are compared with those obtained in the dark for samples 105U (almost symmetric) and 216U (asymmetric). As can be seen, the increase in current due to photoexcitation, albeit small, is clearly observed for positive bias, while for negative bias effects are less evident, especially for device 216U. Low photocurrent gain for heavily doped GaN nanowires was already observed previously [32–34]. A possible explanation for this is that heavy doping limits the depletion width in dark environment to already very small values. Consequently, irradiation with UV light will not drastically improve the electron transport through the wire as it does, for example, in fully depleted wires [32]. The fact that we obtained a higher gain factor when the more ohmic like contact dictates the behaviour (i.e. when it is polarized in reverse bias) of the device is surprising, as typically a lower dark current is more advantageous in terms of detection efficiency. A possible reason for this is the existence of the SiN_x shell at the n++ extremity, which is not present at the n extremity and may improve the detection efficiency. However, due to the size of the devices, which are smaller than the spot size of the used light source, we cannot say with certainty if the UV detection occurs mainly in the depletion region formed at the metal-semiconductor interface or in the depletion region created by the surface states of the wires. Consequently, to address this issue, a deeper analysis of the detection mechanism must be made in future work.

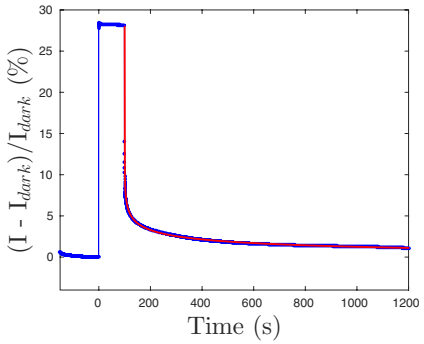

Figure 6. Transient I–V curve measured with device 216U for a bias of 3 V; the light was turned on at $t = 0$ s and off at $t = 100$ s; the blue line corresponds to the experimental data and the red line corresponds to the fit of the decay. The y-axis corresponds to the current gain calculated according $100 \times (I(t) - I_{\text{dark}})/I_{\text{dark}}$.

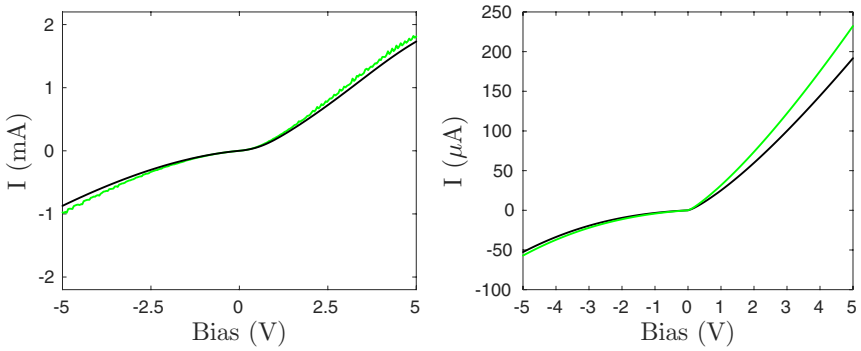

Figure 7. I–V characteristics, for the same devices (105U and 216U) as measured in figures 5(a) and (b), measured under dark (black curve) conditions and when irradiated with protons (green curve). We notice that the dark current for sample 216U has decreased by 60% in comparison to the dark current during photoconductivity measurements since this device was already exposed to some irradiation before performing the measurement.

In figure 6 a transient measurement done with the device 216U at a 3 V bias is shown. After turning the light on, the current increases abruptly and then stabilizes with a gain factor of approximately 28%. Once the current reaches a stable value the light is turned off again. To extract the decay time, the data was fitted using the following equation [35]

$$\Delta I = \Delta I_{\text{uv}} \exp\left[-\left(\frac{t}{\tau_d}\right)^{\beta}\right], \qquad (1)$$

where, $\Delta I = (I(t) - I_{\text{dark}})/I_{\text{dark}}$, $\Delta I_{\text{uv}} = (I_{\text{uv}} - I_{\text{dark}})/I_{\text{dark}}$, the decay time is given by τ_d and β represents the exponential stretching parameter.

The obtained decay time for the presented curve is 0.88 ± 0.01 s while the exponential stretching parameter yielded 0.1510 ± 0.0004. The values obtained for other devices and with different applied bias in the range of 1 to 4 V are of the same order. The values obtained for β are in agreement with some of the previously reported results for both GaN thin films and nanowires [36, 37]. Higher values of beta (usually a sign of less defective crystals) have been reported for GaN films measured by contactless microwave probed photoconductivity [38]. The low beta values found here for wires with high crystalline quality may therefore be due to defects formed in the contact regions.

Regarding τ_d, for a typical photodetector, a decay time of the order of a second is quite large. The long times are a consequence of the effects of PPC, which have been widely reported in GaN thin film and nanowire devices. Decay times obtained for c-axial nanowires with a diameter of 500 nm were longer than 120 s [4] and for MBE grown thin films around 130 s [39]. Photocurrent decay studies were also performed with the same kind of microwires as used in this investigation, but containing five core-shell InGaN/GaN multiquantum wells. The obtained decay time was of the order of 3000 s and the exponential stretching factor yielded 0.35 [40]. Compared to these results our decay times are thus relatively fast. In a-plane GaN thin films similar decay times have been observed as obtained here [41]. Nonetheless, the best values regarding the decay time, 26 ms, were obtained with a-axial GaN nanowires [42]. The fast response was attributed to the used Schottky configuration which was also implemented in this work and can therefore partly explain our results relative to the reports where a different configuration was used. Additionally, the superior crystalline quality of microwires when compared to thin films and reduced influence of the surface when compared to nanowires can also improve the response times.

3.3. Proton irradiation

The following step in the study of the sensors consists of exposing them to proton irradiation to test their radiation resistance and applicability as particle detectors. The first experiments consisted of measuring the change in current due to the ionizing irradiation. In figure 7(a) we compare the obtained I–V curves for sample 105U in the dark and when irradiating it with protons. We observe that the result is very similar as that obtained during photoconductivity measurements. In figure 7(b) we show the same measurement for device 216U. In this case, the sample had been already exposed to radiation with a fluence of 7.4×10^{16} protons cm^{-2} prior to the measurement which caused a decrease in the dark current. In comparison to the dark current shown in figure 5(b), it decreased by 60%.

When exposing the sample to protons, we observe a slightly higher increase in current for positive bias compared to the photoconductivity measurement of the unirradiated device, while maintaining a small gain at negative bias. The fact that we did not observe this for sample 105U suggests that the lower dark current has a significant influence on the higher gain. However, the higher excitation density and excitation depth for proton irradiation may also play a role.

To verify the effects of the irradiation on the overall performance of the devices, two devices were continuously exposed to protons for a longer time interval. At the same time, their I–V characteristics were being measured continuously. The ensemble of I–V curves is represented in figure 8(a). The resistance for some curves was estimated by fitting the linear region which typically exists between between 3 V and 5 V. The data shows an increase from approximately 1 kΩ before exposure to irradiation, to over 120 kΩ after 150 s of exposure

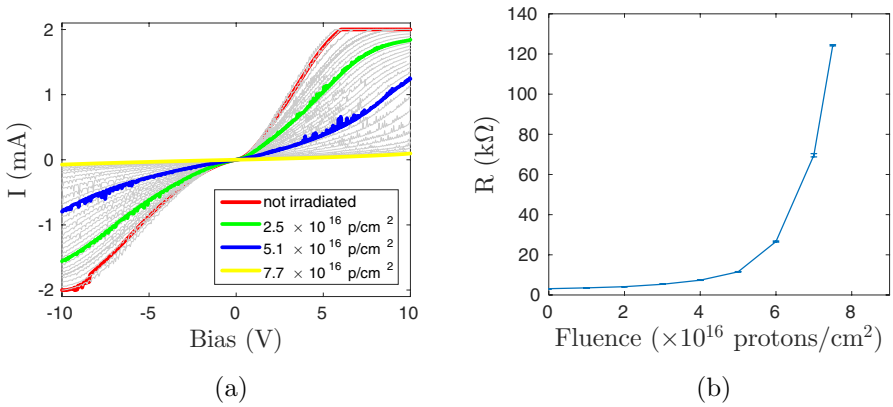

Figure 8. (a) The I–V curves of sample 105U taken while being exposed to proton radiation. The legend indicates the fluences of the coloured curves. The saturation at high voltage is a consequence of the limitation of the current compliance to 2 mA, which was set at this value to protect the devices; (b) the resistance plotted versus the proton fluence.

to irradiation with a total fluence of 7.5×10^{16} protons cm^{-2} as can be seen in figure 8(b). The decay in conductivity is a consequence of the creation of defect levels in the bandgap by the irradiation. Additional acceptor states will trap electrons and decrease the carrier concentration [43]. On the other hand, at the metal-semiconductor interfaces, the Schottky barrier heights typically increase [44] which can drastically change the preferential mechanism of electron transport through the device. Nevertheless, the strong increase of resistance for the majority of the devices only starts at fluences above $\sim 4 \times 10^{16}$ protons cm^{-2}, which confirms the high radiation resistance of GaN devices. In fact, for proton irradiation of thin film devices under similar conditions, a strong decrease of the exponential stretching factor in transient measurements has been reported already for two magnitudes lower proton fluences [38]. As shown below, this is not the case for the microwire devices pointing to increased radiation resistance possibly due to the low density of native defects which can interact with irradiation induced defects.

The decay in conductivity as a consequence of irradiation makes it harder to perform stable transient I–V measurements. However, since the response time of our devices is relatively fast, this could be overcome by only turning the beam on for a short time, short enough to avoid significant defect creation and long enough to reach the saturation current. The obtained curve for sample 229U is depicted in figure 9. The final dark current is still below the initial dark current, but the difference is small. Equation (1) was used again to fit the curve and the resulting decay time is $\tau_d = 0.628 \pm 0.009$ s, with a stretching parameter of $\beta = 0.2293 \pm 0.0008$. Transient photoconductivity measurements prior to the irradiation done on the same sample yielded $\tau_d = 3.97 \pm 0.02$ with $\beta = 0.2117 \pm 0.0002$. Results obtained by Johannes *et al* when irradiating ZnO nanowires with He^+ ions yielded an increase in current of approximately 400% during a first implantation and an increase in current of approximately 100% during a second implantation [9]. The current increase in our case is thus significantly lower. Nonetheless, the decay time of the persistent ion beam induced current in the case of the ZnO nanowires is significantly larger, and especially slow when the sample is subjected to vacuum. Typically, band

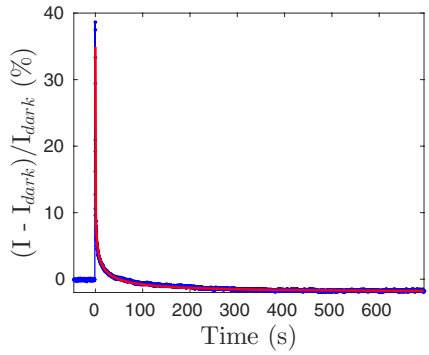

Figure 9. Transient I–V curve with an applied bias of 3 V representing the response to proton radiation after a short pulse for sample 229U. The blue line corresponds to the experimental data and the red line corresponds to the fit result.

bending due to surface defects causes the adsorption of O_2 molecules at the surface which desorb during the measurement and persistent currents are strongly enhanced when the measurement is done in vacuum [9, 45]. In our samples we do not verify this effect, since decay times during the photoconductivity measurements (done in ambient atmosphere) and proton measurements (done in vacuum) are of the same order of magnitude. This suggests that surface states do not play a major role in the processes that govern the current decay after excitation.

3.4. Proton irradiation effects on photoconductivity

As observed, the ionizing radiation has severe consequences on the overall conductivity of the sensors. It is therefore interesting to redo the photoconductivity measurements in order to see whether the response of the devices is maintained. This was done for device 216U which was irradiated with a total fluence of 1.2×10^{17} protons cm^{-2}. To recover some of the defects created by the proton irradiation, first an annealing step at 600 °C for 120 s was done in flowing nitrogen atmosphere. We compared the dark current measured immediately after the proton irradiation and the dark current after the annealing step with the dark current prior to the irradiation. The current after irradiation represented 7% of the initial dark current where

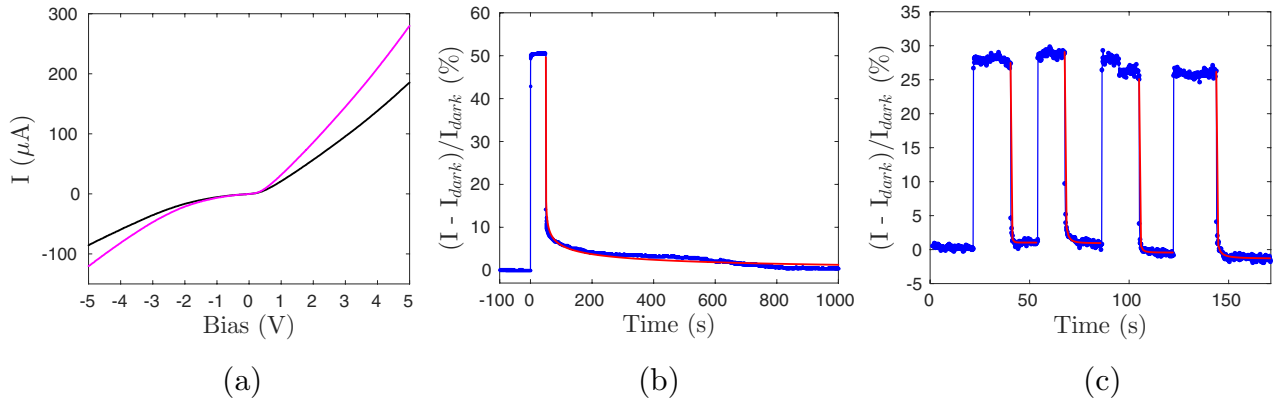

Figure 10. (a) I–V curves for sample 216U after irradiation with a total proton fluence of 1.18×10^{17} protons cm^{-2} and rapid thermal annealing, while illuminating the device with UV light, are shown. The black curve corresponds to I_{dark} and the magenta curve to I_{uv}; (b) transient I–V measurement performed at a bias of 3 V with sample 216U; (c) transient I–V measurements at -3 volts for the 216U device. Since the decay time for negative bias is fast, the UV light was turned on and off several times. The blue dots correspond to the experimental data and the red lines to the respective fits.

after annealing the current represented 12% of the initial dark current. We note that no measurable alterations in the contact properties were observed for such annealing conditions in unirradiated devices. Then, the same I–V measurements as prior to the irradiation were done (see figures 5(b) and 6). The obtained results are shown in figures 10(a) and 10(b).

If we compare the responsivity of the devices to the UV light before and after the irradiation, we can see that it has been improved for the latter case. Prior to the irradiation, the gain at a bias of 3 V was $28.13 \pm 0.04\%$ while afterwards it increased significantly to a value of $50.6 \pm 0.5\%$. The most significant difference is seen for negative bias though, where prior to the irradiation the gain was negligible, after proton irradiation it reaches values up to 40%. The increase in the photocurrent gain can be explained following the carrier removal due to the defects created by the irradiation. As the amount of carriers in the dark case is now smaller, the amount of excess carriers generated when the excitation occurs, represents a bigger fraction, hence the increased gain factor.

Additionally, the decay time at a bias of -3 V is surprisingly fast as the fit result yields $\tau_d \simeq 0.03$ s, which is one order of magnitude below the decay times at positive bias (see figures 10(b) and (c)). Unfortunately, no measurements at $V < 0$ V could be done before the irradiation due to the low response, so we cannot directly say that the fast decay times are a consequence of the irradiation. Nonetheless, a decrease of the decay time after exposure to protons has been observed previously for thin films [46]. The partial removal of the deep acceptor states by the proton irradiation was suggested as a possible cause because a quenching of the yellow band, typically associated to transitions between deep acceptor states and the conduction band was observed as well while performing photoconductivity spectroscopy measurements after the irradiation [46]. The results of the transient photoconductivity measurements for samples 216U and 210U at a 3 V bias are summarized in table 1 where they are also compared with the results obtained prior to the proton irradiation. We note that the total fluence of the irradiation to which sample 210U was exposed is smaller, 3.2×10^{16} protons cm^{-2}, in comparison to the fluence to which other samples were exposed. This is due to the fact that, for this sample, the decay in current was more pronounced. The difference in decay times, albeit large for sample 210U, can be considered as approximately equal considering that the used model is relatively general such that τ_d and β, in the absence of other supporting evidence, cannot easily be associated with specific material parameters. Regarding the photocurrent gain, ΔI we can clearly see that the results after irradiation are significantly better than before the irradiation for both samples.

Table 1. Results obtained by fitting equation (1) to the obtained curves with transient I–V measurements at $V = 3$ V for samples 210U and 216U with UV excitation, before and after the irradiation with protons. Sample 216U was irradiated with a total fluence of 1.18×10^{17} protons cm^{-2} while sample 210U was irradiated with a total fluence of 3.2×10^{16} protons cm^{-2}.

Sample	Parameter	Before irradiation	After irradiation
210U	τ_d (s)	0.61 ± 0.01	2.04 ± 0.03
	β	0.1828 ± 0.0004	0.1388 ± 0.0005
	ΔI (%)	7.24 ± 0.02	26.71 ± 0.08
216U	τ_d (s)	0.88 ± 0.01	0.55 ± 0.02
	β	0.1510 ± 0.0004	0.1591 ± 0.0009
	ΔI (%)	28.13 ± 0.04	50.6 ± 0.5

4. Conclusions

Radiation sensors based on GaN microwires were processed and their capability to detect UV light and protons demonstrated. The performed opto-electrical characterization revealed a fast response to irradiation with UV light above the GaN bandgap. Minimum decay times below one second were measured which is faster than most previously reported studies on GaN nanowires or thin film based photodetectors. The photocurrent gain of the fabricated photodetectors is, however, still too low to be interesting for application in actual devices. The main cause for this occurrence is probably the high doping concentration, as this leads to a very large dark current.

Our findings based on the proton-irradiation studies of the devices revealed promising results. Measurements performed on an unirradiated sample revealed a similar ionocurrent gain when compared with the photocurrent gain measured with the same device. Ion beam induced current measurements performed on a device that suffered proton irradiation with a fluence of 7.4×10^{16} protons cm^{-2} showed higher current gain factors upon proton irradiation and, after excitation, the time it took the devices to return to the stable dark current was of the same order of magnitude as the photocurrent decay time. These results indicate that GaN microwires have the potential to be applied in particle detectors in the same way as they are already applied in UV photodetectors. Furthermore, our results indicate that GaN microwire devices are even more radiation resistant than their thin film counterparts. Finally, the irradiated devices were annealed and tested again regarding their UV detection potential. The results indicated overall improved responses and the photocurrent gain increased to approximately twice the values obtained prior to the irradiation. Promising results regarding significantly faster photocurrent decay times, $\tau_d \simeq 0.03$ s for a negative bias of -3 V, were also obtained in the proton irradiated samples.

Despite the low gain achieved, the present work provides the proof of principle showing that GaN microwires are promising building blocks for particle detectors. The main restriction for the present device design is due to the high carrier concentrations in MOVPE grown microwires even in the unintentionally doped section. According to previous studies [7, 8] we expect that significant improvements in the device performance can be achieved by using p-n junctions with low carrier concentrations in the depletion layer leading to lower dark currents in reverse bias. The addition of the junction may therefore significantly improve the detection efficiency of the devices as well as supress persistent currents.

Acknowledgments

Financial support by FCT Portugal is gratefully acknowledged: grants UID/FIS/50010/ 2013 and UID/Multi/04349/2013; M Peres acknowledges grant SFRH/BPD/111285/2015 and K Lorenz the program Investigador FCT. The work has been performed within the bilateral collaboration program PESSOA.

ORCID iDs

M Peres https://orcid.org/0000-0001-6774-8492
J Eymery https://orcid.org/0000-0002-4216-1166
K Lorenz https://orcid.org/0000-0001-5546-6922

References

[1] Sang L, Liao M and Sumiya M 2013 *Sensors* **13** 10482–518
[2] Chen Q, Yang J W, Osinsky A, Gangopadhyay S, Lim B, Anwar M Z, Khan M A, Kuksenkov D and Temkin H 1997 *Appl. Phys. Lett.* **70** 2277–9
[3] Rigutti L and Tchernycheva M 2014 GaN nanowire-based ultraviolet photodetectors *Wide Band Gap Semiconductor Nanowires 2: Heterostructures and Optoelectronic Devices* ed V Consonni and G Feuillet (New York: Wiley) pp 179–202
[4] Calarco R, Marso M, Richter T, Aykanat A I, Meijers R, Hart A V D, Stoica T and Lüth H 2005 *Nano Lett.* **5** 981–4
[5] Chen H Y, Chen R S, Rajan N K, Chang F C, Chen L C, Chen K H, Yang Y J and Reed M A 2011 *Phys. Rev.* B **84** 205443
[6] Schlenker E, Bakin A, Weimann T, Hinze P, Weber D H, Gölzhäuser A, Wehmann H H and Waag A 2008 *Nanotechnology* **19** 365707
[7] Zhang H, Messanvi A, Durand C, Eymery J, Lavenus P, Babichev A, Julien F H and Tchernycheva M 2016 *Phys. Status Solidi* A **213** 936–40
[8] Zhang H *et al* 2016 *ACS Appl. Mater. Inter.* **8** 26198–206
[9] Johannes A, Niepelt R, Gnauck M and Ronning C 2011 *Appl. Phys. Lett.* **99** 252105
[10] Polyakov A Y *et al* 2009 *J. Appl. Phys.* **106** 103708
[11] Xu Q, Mulligan P, Wang J, Chuirazzi W and Cao L 2017 *Nucl. Instrum. Methods Phys. Res.* A **849** 11–5
[12] Vaitkus J, Cunningham W, Gaubas E, Rahman M, Sakai S, Smith K and Wang T 2003 *Nucl. Instrum. Methods Phys. Res.* A **509** 60–4
[13] Marques J G, Lorenz K, Franco N and Alves E 2006 *Nucl. Instrum. Methods Phys. Res.* B **249** 358–61
[14] Lorenz K, Peres M, Franco N, Marques J G, Miranda S M C, Magalhaes S, Monteiro T, Wesch W, Alves E and Wendler E 2011 *Proc. SPIE* **7940** 7940O
[15] Grant J, Bates R, Cunningham W, Blue A, Melone J, McEwan F, Vaitkus J, Gaubas E and O'Shea V 2007 *Nucl. Instrum. Methods Phys. Res.* A **576** 60–5
[16] Pearton S J, Deist R, Ren F, Liu L, Polyakov A Y and Kim J 2013 *J. Vac. Sci. Technol.* A **31** 050801
[17] Kozodoy P, Ibbetson J P, Marchand H, Fini P T, Keller S, Speck J S, DenBaars S P and Mishra U K 1998 *Appl. Phys. Lett.* **73** 975–7
[18] Coulon P M, Mexis M, Teisseire M, Jublot M, Vennéguès P, Leroux M and Zuniga-Perez J 2014 *J. Appl. Phys.* **115** 153504
[19] Labat S *et al* 2015 *ACS Nano* **9** 9210–6
[20] Calarco R, Stoica T, Brandt O and Geelhaar L 2011 *J. Mater. Res.* **26** 2157–68
[21] Koester R, Hwang J S, Durand C, Dang D L S and Eymery J 2010 *Nanotechnology* **21** 015602
[22] Tchoulfian P, Donatini F, Levy F, Dussaigne A, Ferret P and Pernot J 2014 *Nano Lett.* **14** 3491–8
[23] Messanvi A *et al* 2015 *ACS Appl. Mater. Interfaces* **7** 21898–906
[24] Brinza M, Willekens J, Benkhedir M and Adriaenssens G 2007 *Photoconductivity in Materials Research* (Boston, MA: Springer) pp 137–46
[25] Ziegler J F, Biersack J P and Littmark U (ed) 1985 *The Stopping and Range of Ion in Solids* (New York: Pergamon) (https://doi.org/10.1007/978-3-642-68779-2_5)
[26] Nord J, Nordlund K, Keinonen J and Albe K 2003 *Nucl. Instrum. Methods Phys. Res.* B **202** 93–9
[27] Sawada T, Kimura N, Imai K, Suzuki K and Tanahashi K 2004 *J. Vac. Sci. Technol.* B **22** 2051–8
[28] Zhang Z, Yao K, Liu Y, Jin C, Liang X, Chen Q and Peng L M 2007 *Adv. Funct. Mater.* **17** 2478–89
[29] Neaman D A (ed) 2003 *Semiconductor Physics and Devices* 3rd edn (New York: McGraw-Hill)
[30] Tchoulfian P, Donatini F, Levy F, Amstatt B, Ferret P and Pernot J 2013 *Appl. Phys. Lett.* **102** 122116
[31] Tchoulfian P, Donatini F, Levy F, Amstatt B, Dussaigne A, Ferret P, Bustarret E and Pernot J 2013 *Appl. Phys. Lett.* **103** 202101
[32] González-Posada F, Songmuang R, Den Hertog M and Monroy E 2012 *Nano Lett.* **12** 172–6
[33] Richter T, Meijers H, Lüth R, Calarco R and Marso M 2008 *Nano Lett.* **8** 3056–9

[34] Rigutti L, Tchernycheva M, Bugallo A L, Jacopin G, Julien F H, Zagonel L F, March K, Stephan O, Kociak M and Songmuang R 2010 *Nano Lett.* **10** 2939–43
[35] Qiu C H and Pankove J I 1997 *Appl. Phys. Lett.* **70** 1983–5
[36] Li J Z, Lin J Y, Jiang H X, Salvador A, Botchkarev A and Morkoc H 1996 *Appl. Phys. Lett.* **69** 1474–6
[37] Chen H M, Chen Y F, Lee M C and Feng M S 1997 *J. Appl. Phys.* **82** 899–901
[38] Gaubas E, Ceponis T, Jasiunas A, Kovalevskij V, Meskauskaite D, Pavlov J, Remeikis V, Tekorius A and Vaitkus J 2014 *Appl. Phys. Lett.* **104** 062104
[39] Winnerl A, Pereira R N and Stutzmann M 2015 *Phys. Rev.* B **91** 075316
[40] Bugallo A L, Rigutti L, Jacopin G, Julien F H, Durand C, Chen X J, Salomon D, Eymery J and Tchernycheva M 2011 *Appl. Phys. Lett.* **98** 233107
[41] Gundimeda A, Krishna S, Aggarwal N, Sharma A, Sharma N D, Maurya K K, Husale S and Gupta G 2017 *Appl. Phys. Lett.* **110** 103507
[42] Wang X, Zhang Y, Chen X, He M, Liu C, Yin Y, Zou X and Li S 2014 *Nanoscale* **6** 12009
[43] Titov A I, Karasev P A and Kucheyev S O 2004 *Semiconductors* **38** 1179–86
[44] White B D, Bataiev M, Goss S H, Hu X, Karmarkar A, Fleetwood D M, Schrimpf R D, Schaff W J and Brillson L J 2003 *IEEE Trans. Nucl. Sci.* **50** 1934–41
[45] Pereira D, Peres M, Alves L, Correia J, Díaz-Guerra C, Silva A, Alves E and Lorenz K 2018 *Surf. Coat. Technol.* (https://doi.org/10.1016/j.surfcoat.2018.01.034)
[46] Castaldini A, Cavallini A and Polenta L 2005 *Phys. Status Solidi* A **202** 2912–9